Supporting Material

UNEXPECTED MULTIPLE ACTIVATED STEPS IN THE EXCITED STATE DECAY OF SOME *BIS*(PHENYLETHYNYL)-FLUORENES AND –ANTHRACENES

G. Cacioppa, B. Carlotti, F. Elisei, P.L. Gentili, A. Marrocchi and A. Spalletti

Department of Chemistry, Biology and Biotechnology and Centro di Eccellenza sui Materiali Innovativi Nanostrutturati (CEMIN) University of Perugia, via Elce di Sotto 8, 06123 Perugia (Italy)

E-mail: anna.spalletti@unipg.it

SI1. Temperature effect on the spectral behavior

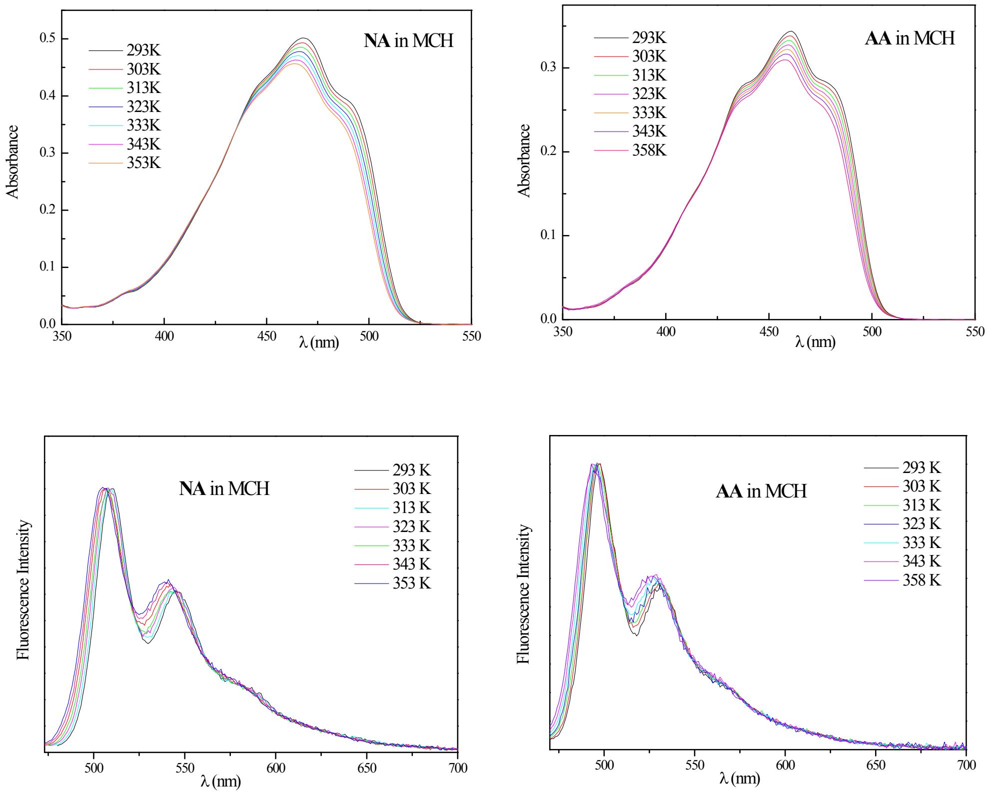

Fig. S1 Absorption (upper) and normalized emission (bottom) spectra of **NA** and **AA** in MCH as a function of temperature.

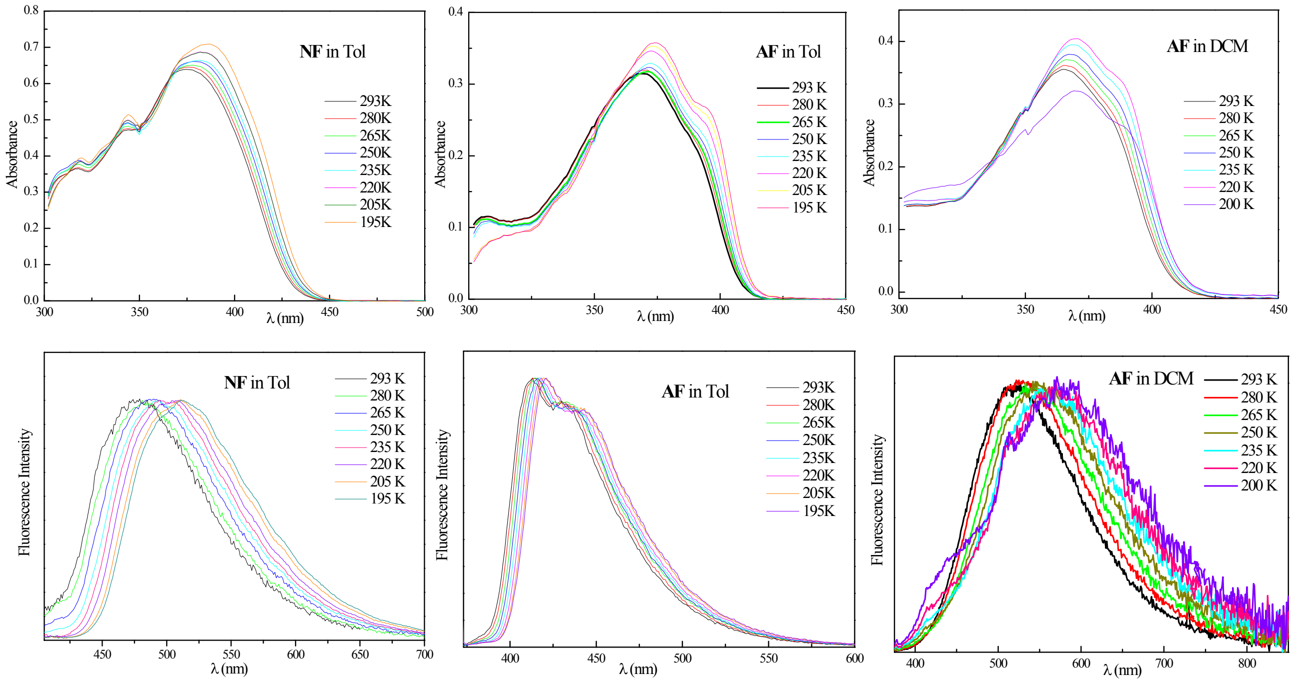

Fig. S2 Absorption (upper) and normalized emission (bottom) spectra of **NF** in Tol and **AF** in Tol and DCM at different temperatures.

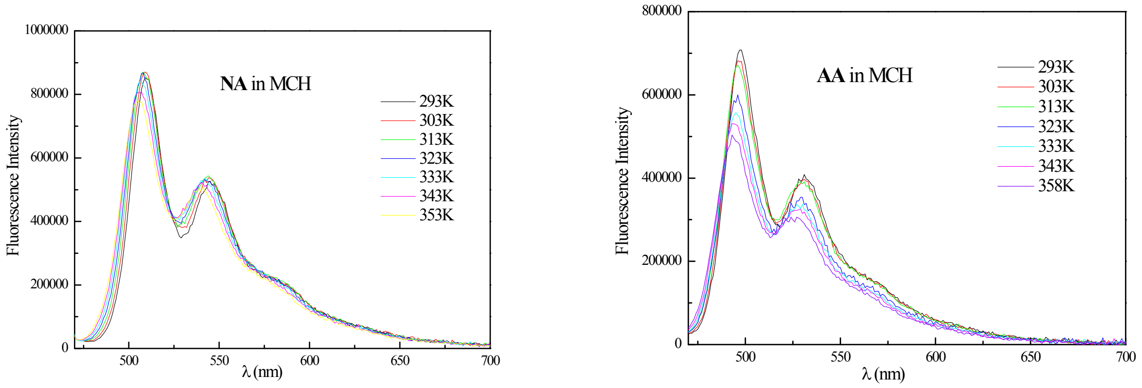

Fig. S3 Non-normalized emission spectra of **NA** and **AA** in MCH as a function of temperature.

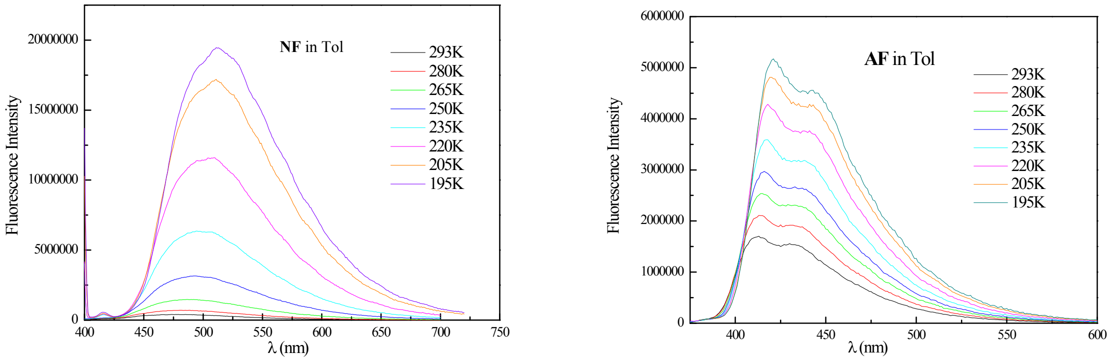

Fig. S4 Non-normalized emission spectra of **NF** and **AF** in Tol as a function of temperature.

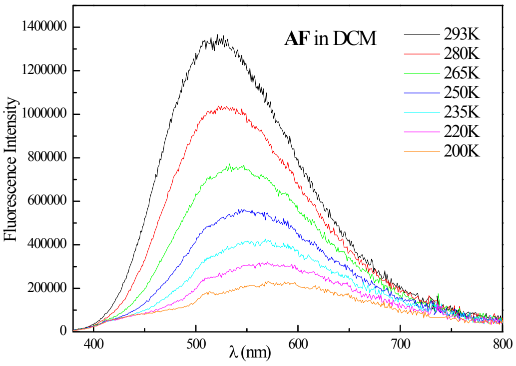

Fig. S5 Non-normalized emission spectra of **AF** in DCM as a function of temperature.

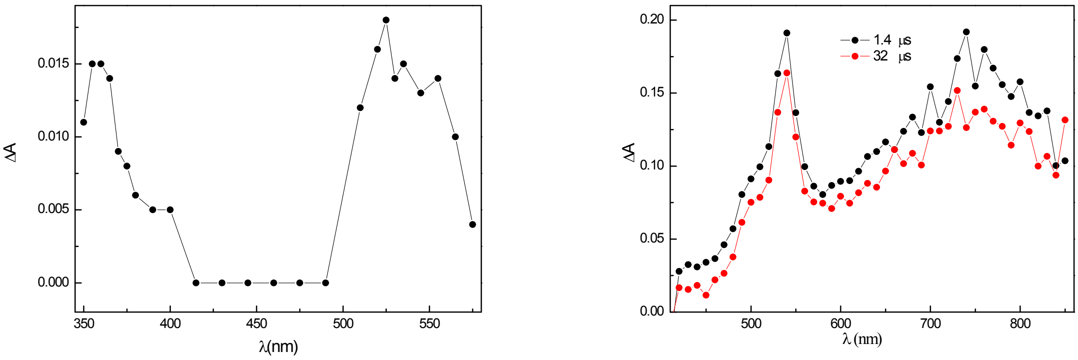

Fig. S6 $T_1 \rightarrow T_n$ absorption spectrum of **AA** in MCH at 358 K (left) and **AF** in Tol at 195 K at different delays after the laser pulse (right).

SI2. MEM analysis of decay kinetics

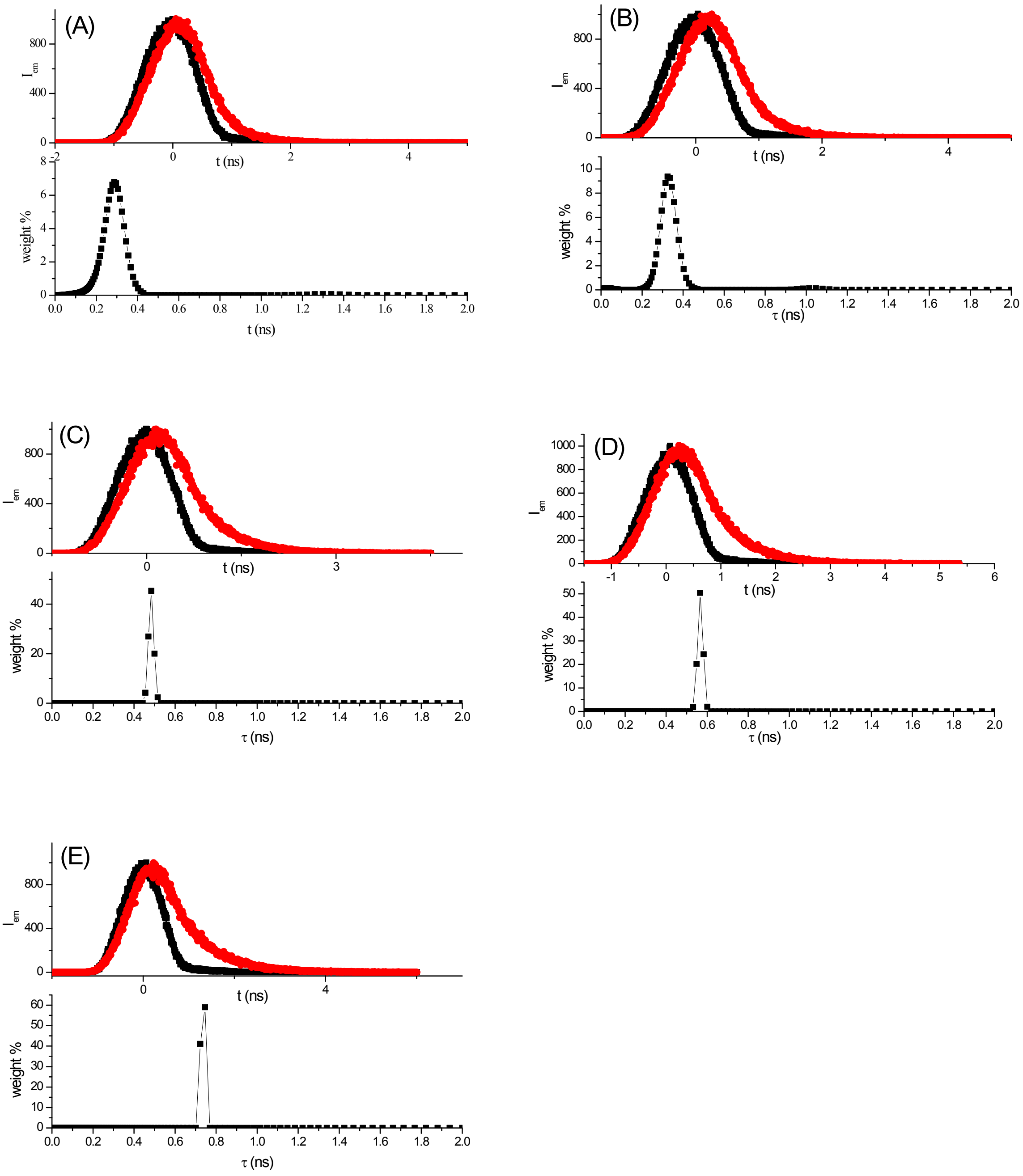

Fig. S7 AF in Tol at 293 K (A), 280 K (B), 250 K (C), 235 K (D), and 205 K (E). The top parts of the graphs show the profiles of the decay (red traces) and prompt (black traces), whereas the bottom parts show the output of the MEM analysis.

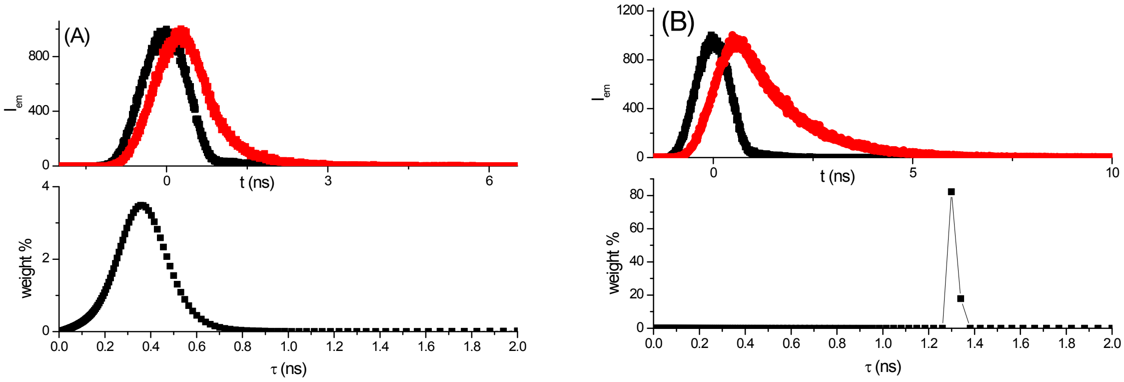

Fig. S8 NF in Tol at 250 K (A) and 220 K (B). The top parts of the graphs show the profiles of the decay (red traces) and prompt (black traces), whereas the bottom parts show the output of the MEM analysis.

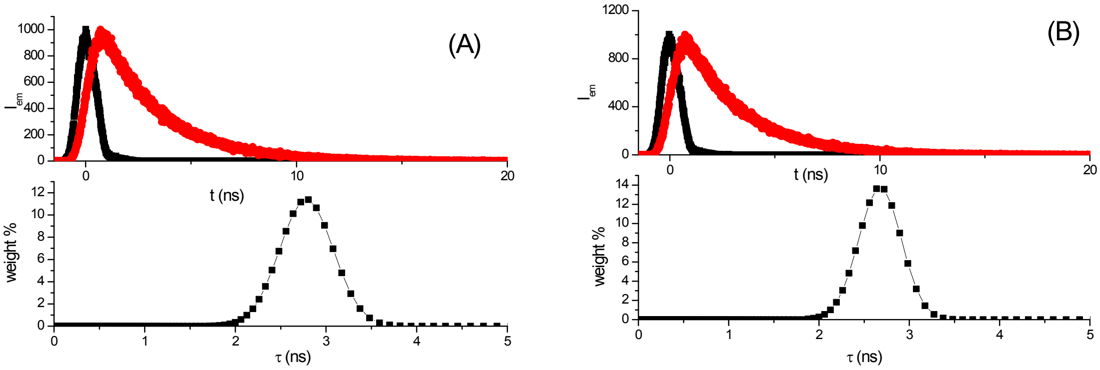

Fig. S9 NA in MCH at 353 K (A) and 293 K (B). The top parts of the graphs show the profiles of the decay (red traces) and prompt (black traces), whereas the bottom parts show the output of the MEM analysis.

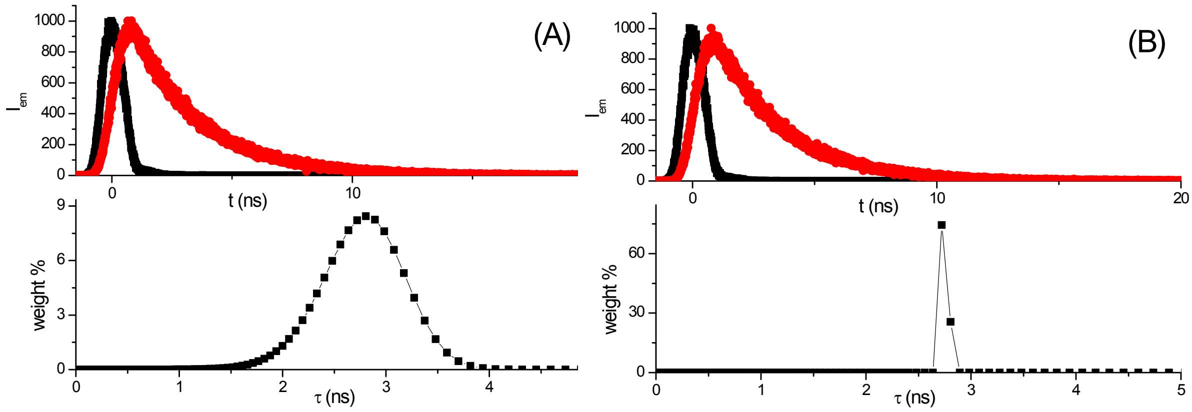

Fig. S10 AA in MCH at 358 K (A) and 293 K (B). The top parts of the graphs show the profiles of the decay (red traces) and prompt (black traces), whereas the bottom parts show the output of the MEM analysis.

SI3. Experimental data fittings

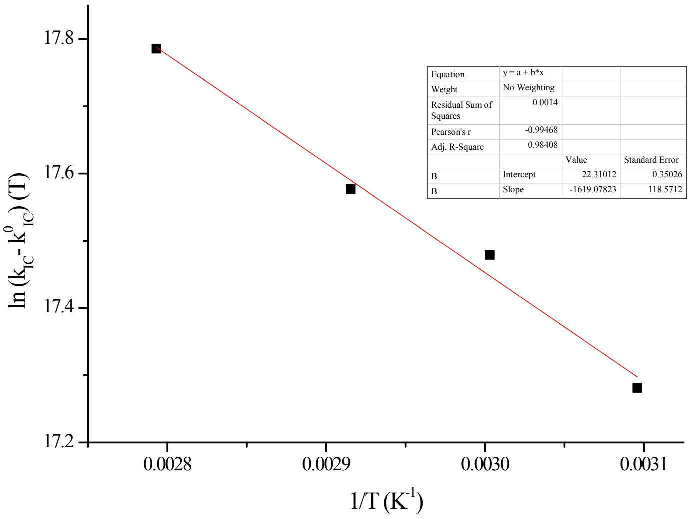

Equation	y = a + b*x		
Weight	No Weighting		
Residual Sum of Squares	0.0014		
Pearson's r	-0.99468		
Adj. R-Square	0.98408		
		Value	Standard Error
B	Intercept	22.31012	0.35026
B	Slope	-1619.07823	118.5712

Fig. S11 Fitting of ln k_{IC} against 1/T according to eq. 1 for **AA** in MCH, by fixing $k_{IC}^{0} =$ 3.5×10^{7} s^{-1}.

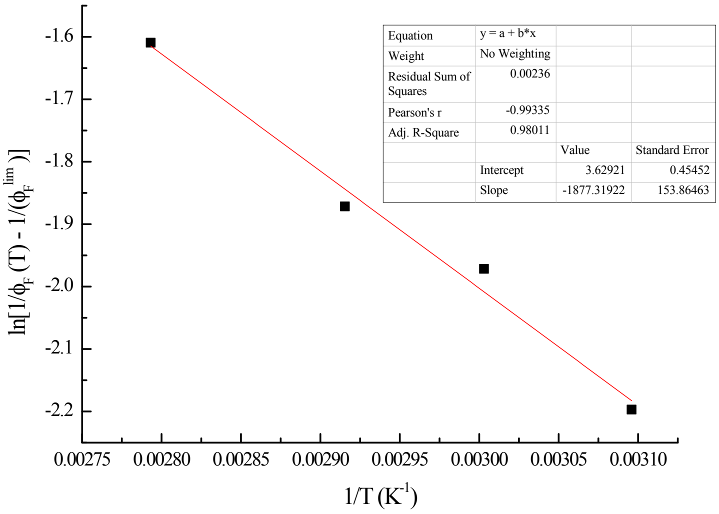

Equation	y = a + b*x		
Weight	No Weighting		
Residual Sum of Squares	0.00236		
Pearson's r	-0.99335		
Adj. R-Square	0.98011		
		Value	Standard Error
	Intercept	3.62921	0.45452
	Slope	-1877.31922	153.86463

Fig. S12 Fitting of $ln[1/\phi_F(T)]$ against 1/T according to eq. 3 for **AA** in MCH, by fixing $\phi_{F}^{lim} =$ 0.9.

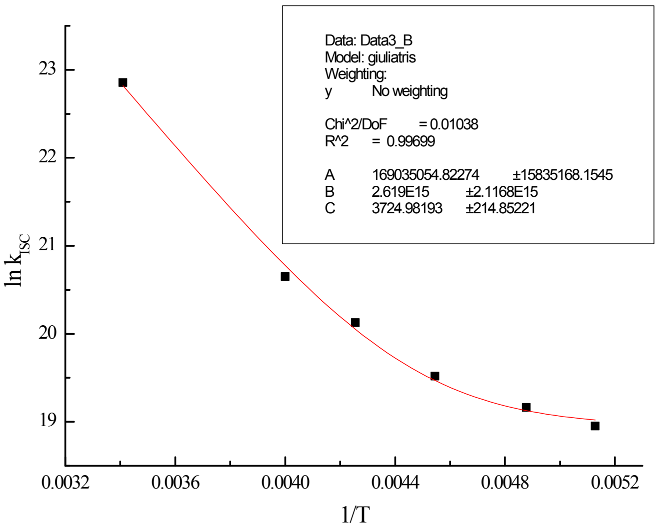

Data: Data3_B
Model: giuliatris
Weighting:
y No weighting

Chi^2/DoF = 0.01038
R^2 = 0.99699

A	169035054.82274	±15835168.1545
B	2.619E15	±2.1168E15
C	3724.98193	±214.85221

Fig. S13 Fitting of ln k_{ISC} against 1/T according to eq. 1 for **NF** in Tol (the fitting parameters A, B and C being k_{ISC}^{0}, A and $E_{a,ISC}/RT$, respectively).

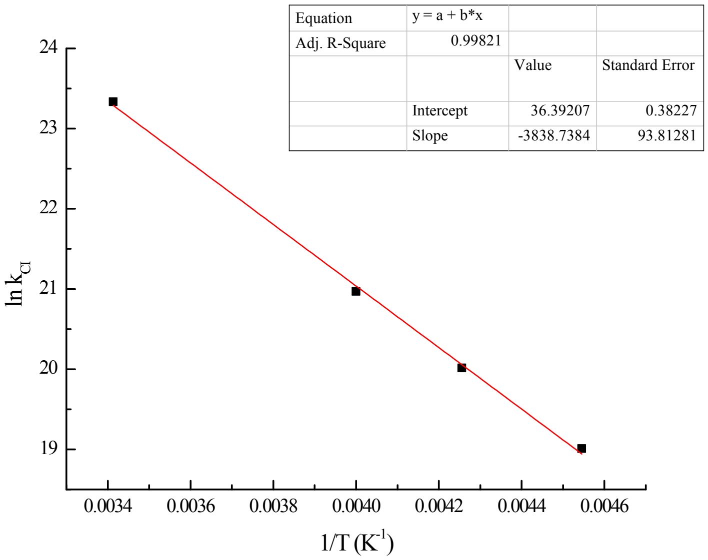

Equation	y = a + b*x		
Adj. R-Square	0.99821		
		Value	Standard Error
	Intercept	36.39207	0.38227
	Slope	-3838.7384	93.81281

Fig. S14 Fitting of ln k_{IC} against 1/T according to eq. 2 for **NF** in Tol.

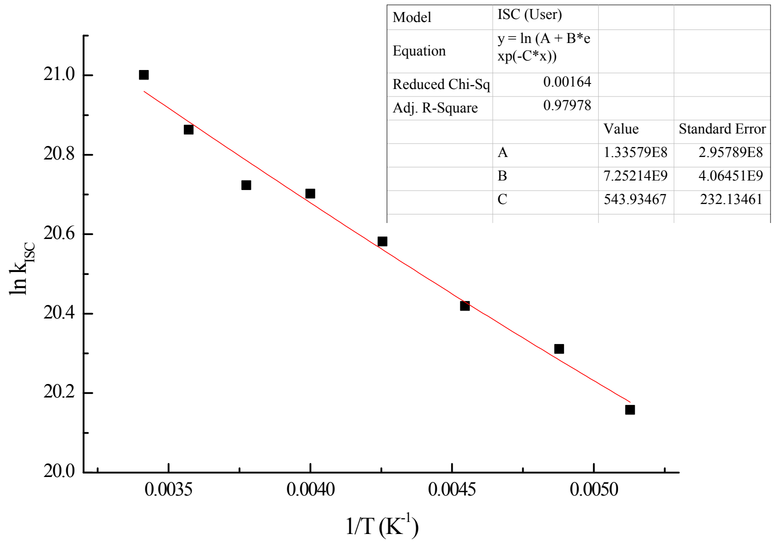

Model	ISC (User)		
Equation	y = ln (A + B*e xp(-C*x))		
Reduced Chi-Sq	0.00164		
Adj. R-Square	0.97978		
		Value	Standard Error
	A	1.33579E8	2.95789E8
	B	7.25214E9	4.06451E9
	C	543.93467	232.13461

Fig. S15 Fitting of ln k_{ISC} against 1/T according to eq. 1 for **AF** in Tol (the fitting parameters A, B and C being k_{ISC}^{0}, A and $E_{a,ISC}/RT$, respectively).

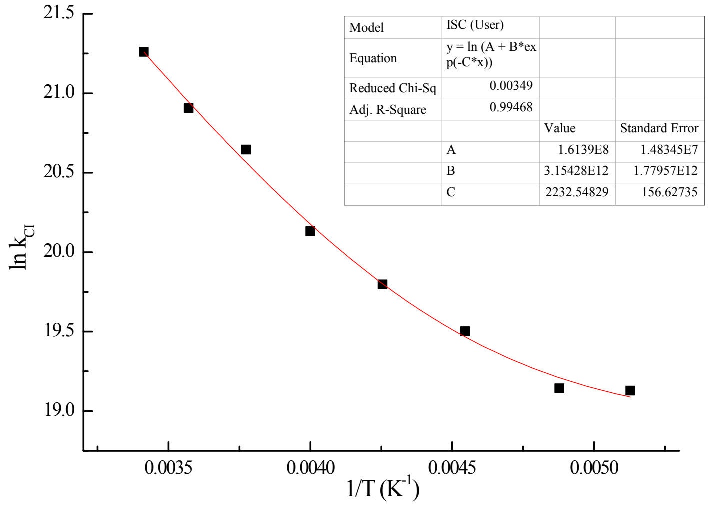

Model	ISC (User)		
Equation	y = ln (A + B*ex p(-C*x))		
Reduced Chi-Sq	0.00349		
Adj. R-Square	0.99468		
		Value	Standard Error
	A	1.6139E8	1.48345E7
	B	3.15428E12	1.77957E12
	C	2232.54829	156.62735

Fig. S16 Fitting of ln k_{IC} against 1/T according to eq. 1 for **AF** in Tol (the fitting parameters A, B and C being k_{IC}^{0}, A and $E_{a,IC}/RT$, respectively).

SI4. Quantum mechanical calculations.

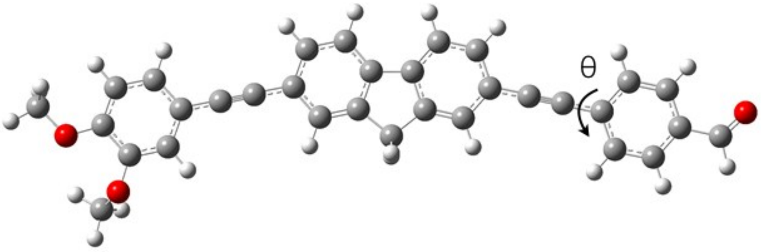

Chart S1 Molecular structure of the ground state of **AF** as optimized by HF in Tol.

Table S1. Transition energy, nature and oscillator strength (f) of the lowest excited singlet and triplet states of **AF** in Tol obtained by TDDFT/B3LYP calculation after HF optimisation of the ground state; the 6-31G(d) basis set was used in all cases.

Excited state	**Transition energy /eV**	**λ /nm**	**Nature**	**%**	**f**
T_1	2.3831	520	$\pi_{H}\rightarrow\pi_{L}^{*}$	55	0.0000
T_2	2.7818	446	$\pi_{H}\rightarrow\pi_{L+1}^{*}$	41	0.0000
S_1	3.0019	413	$\pi_{H}\rightarrow\pi_{L}^{*}$	96	1.5879
T_3	3.2302	384	$n_{H-5}\rightarrow\pi_{L}^{*}$	75	0.0000
T_4	3.3051	375	$\pi_{H-1}\rightarrow\pi_{L+1}^{*}$	32	0.0000
T_5	3.3473	370	$\pi_{H}\rightarrow\pi_{L}^{*}$	43	0.0000
S_2	3.6363	341	$\pi_{H-1}\rightarrow\pi_{L}^{*}$	71	1.0554
S_3	3.7238	333	$n_{H-5}\rightarrow\pi_{L}^{*}$	82	0.0000
S_4	3.7410	331	$\pi_{H}\rightarrow\pi_{L+1}^{*}$	73	0.2387
T_6	3.8021	326	$\pi_{H-2}\rightarrow\pi_{L+1}^{*}$	11	0.0000
T_7	3.8961	318	$\pi_{H}\rightarrow\pi_{L+2}^{*}$	58	0.0000
T_8	3.9240	316	$\pi_{H-8}\rightarrow\pi_{L}^{*}$	76	0.0000
T_9	3.9614	313	$\pi_{H-3}\rightarrow\pi_{L}^{*}$	53	0.0000
T_{10}	4.0602	305	$\pi_{H}\rightarrow\pi_{L+5}^{*}$	16	0.0000
T_{11}	4.0808	304	$\pi_{H}\rightarrow\pi_{L+5}^{*}$	48	0.0000
T_{12}	4.1701	297	$\pi_{H-6}\rightarrow\pi_{L}^{*}$	42	0.0000
T_{13}	4.2879	289	$\pi_{H-1}\rightarrow\pi_{L+1}^{*}$	45	0.0000
S_5	4.2896	289	$\pi_{H}\rightarrow\pi_{L+2}^{*}$	63	0.0077
T_{14}	4.3068	288	$\pi_{H-2}\rightarrow\pi_{L}^{*}$	24	0.0000
S_6	4.3377	286	$\pi_{H-1}\rightarrow\pi_{L+1}^{*}$	37	0.0163

Table S2. Transition energy, nature and oscillator strength (f) of the lowest excited singlet and triplet states of **AF** in DCM obtained by TDDFT/B3LYP calculation after HF optimisation of the ground state; the 6-31G(d) basis set was used in all cases.

Excited state	Transition energy /eV	λ /nm	Nature	%	f
T_1	2.1013	590	$\pi_H \rightarrow \pi^*_L$	60	0.0000
T_2	2.5225	491	$\pi_H \rightarrow \pi^*_{L+1}$	44	0.0000
S_1	2.7487	451	$\pi_H \rightarrow \pi^*_L$	97	1.7178
T_3	3.1007	400	$\pi_H \rightarrow \pi^*_L$	30	0.0000
T_4	3.1074	399	$n_{H-5} \rightarrow \pi^*_L$	75	0.0000
T_5	3.1262	397	$\pi_{H-1} \rightarrow \pi^*_{L+1}$	30	0.0000
S_2	3.4031	364	$\pi_{H-1} \rightarrow \pi^*_L$	69	1.0630
S_3	3.5433	350	$\pi_H \rightarrow \pi^*_{L+1}$	70	0.2150
S_4	3.5921	345	$n_{H-5} \rightarrow \pi^*_L$	82	0.0000
T_6	3.6521	339	$\pi_{H-2} \rightarrow \pi^*_{L+1}$	13	0.0000
T_7	3.7382	332	$\pi_{H-7} \rightarrow \pi^*_L$	59	0.0000
T_8	3.7460	331	$\pi_{H-3} \rightarrow \pi^*_L$	35	0.0000
T_9	3.7885	327	$\pi_H \rightarrow \pi^*_{L+3}$	33	0.0000
T_{10}	3.8705	320	$\pi_{H-2} \rightarrow \pi^*_L$	29	0.0000
T_{11}	3.9700	312	$\pi_H \rightarrow \pi^*_{L+5}$	61	0.0000
T_{12}	4.0082	309	$\pi_{H-6} \rightarrow \pi^*_L$	44	0.0000
T_{13}	4.1006	302	$\pi_{H-1} \rightarrow \pi^*_{L+1}$	43	0.0000
S_5	4.1160	301	$\pi_{H-2} \rightarrow \pi^*_L$	56	0.0146
T_{14}	4.1253	301	$\pi_{H-9} \rightarrow \pi^*_L$	80	0.0000
T_{15}	4.1305	300	$\pi_{H-2} \rightarrow \pi^*_L$	19	0.0000

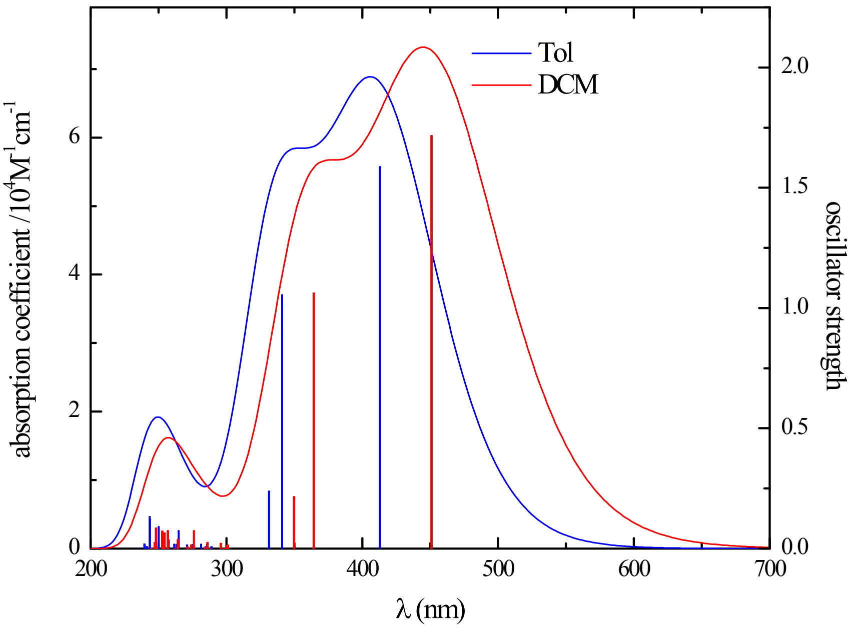

Fig. S17 Absorption spectra of **AF** obtained by TDDTF/B3LYP calculation after HF optimisation of the ground state; the 6-31G(d) basis set was used in all cases.

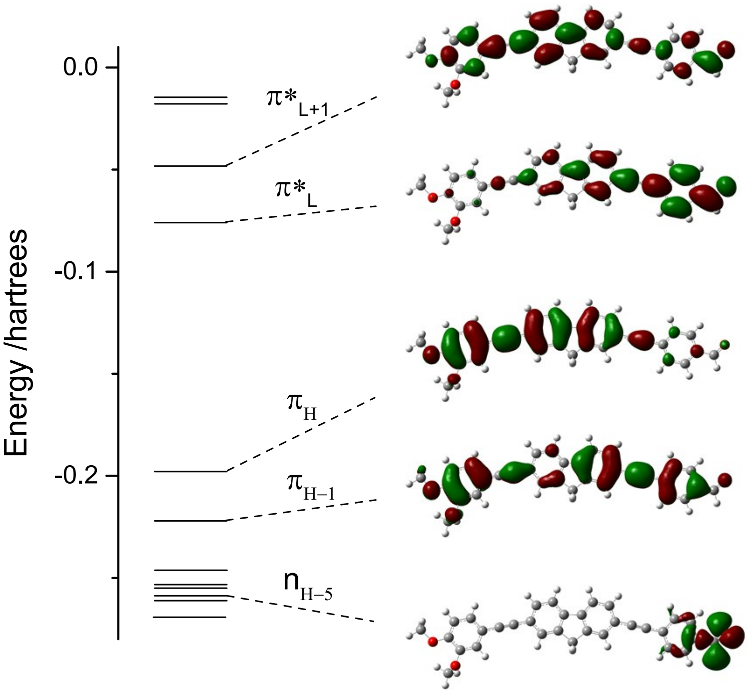

Fig. S18 Most relevant frontier *molecular* orbitals of **AF** in Tol obtained by B3LYP/6-31G(d).

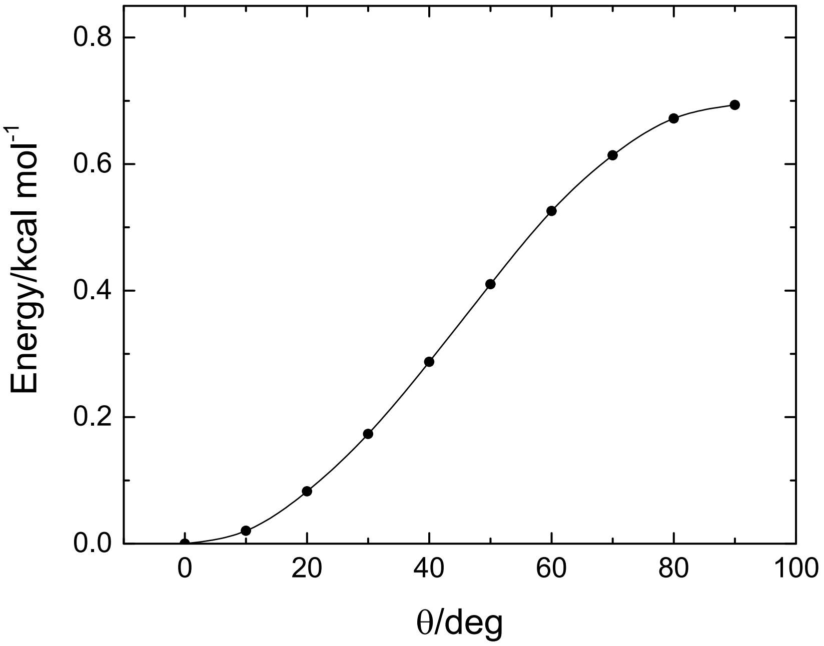

Fig. S19 Effect of the dihedral angle θ (Chart S1) on the energy of **AF** in Tol obtained by HF/6-31G(d).

Table S3. Energies (in eV) of the S_1 and S_2 states of two conformers (θ = 0 and 90 deg, Chart S1) of **AF** in Tol calculated by TDDFT/B3LYP model after HF optimisation of the ground state (the 6-31G(d) basis set was used in all cases).

State	**Nature**	**θ = 0 deg**	**θ = 90 deg**
S_1	π,π^*	3.7240	3.9673
S_2	n,π^*	3.9895	3.9971

SI5. Up-conversion measurements

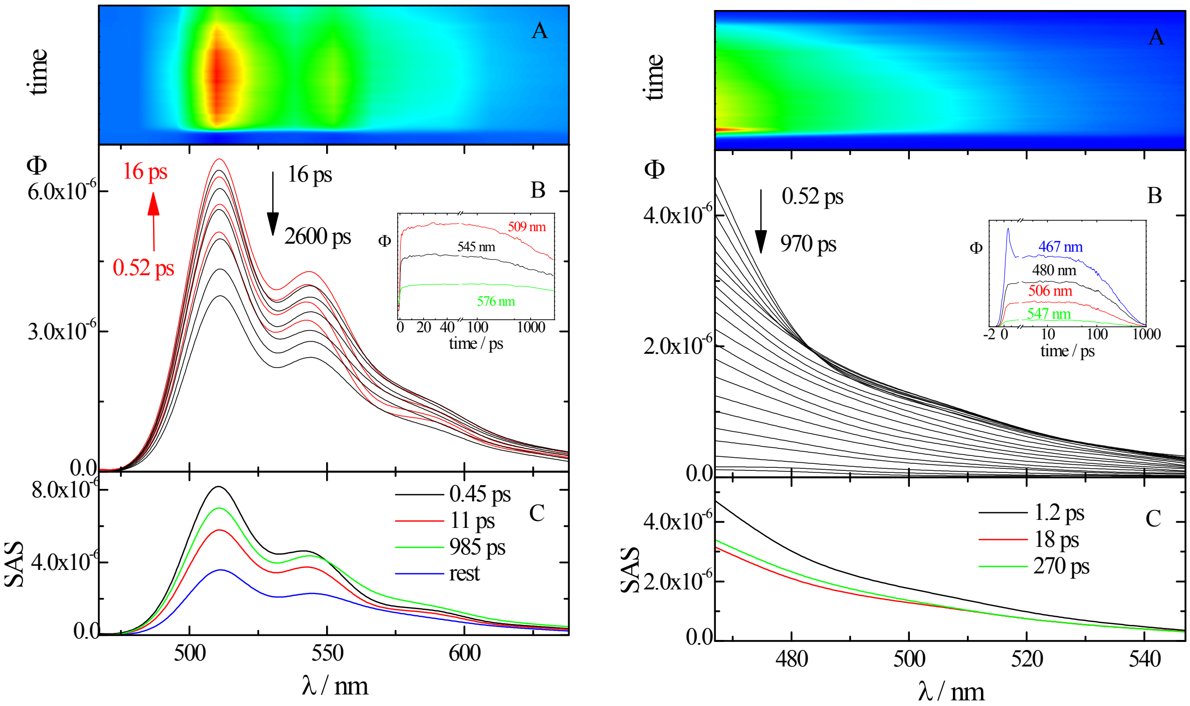

Fig. S20 Fluorescence up−conversion (λ_{exc}=400 nm) of **NA** in CH (left) and **AF** in Tol (right): A) contour plot of the experimental data, B) time resolved emission spectra. Inset: decay kinetics recorded at meaningful wavelengths and C) SAS of the decay components obtained by Target Analysis.

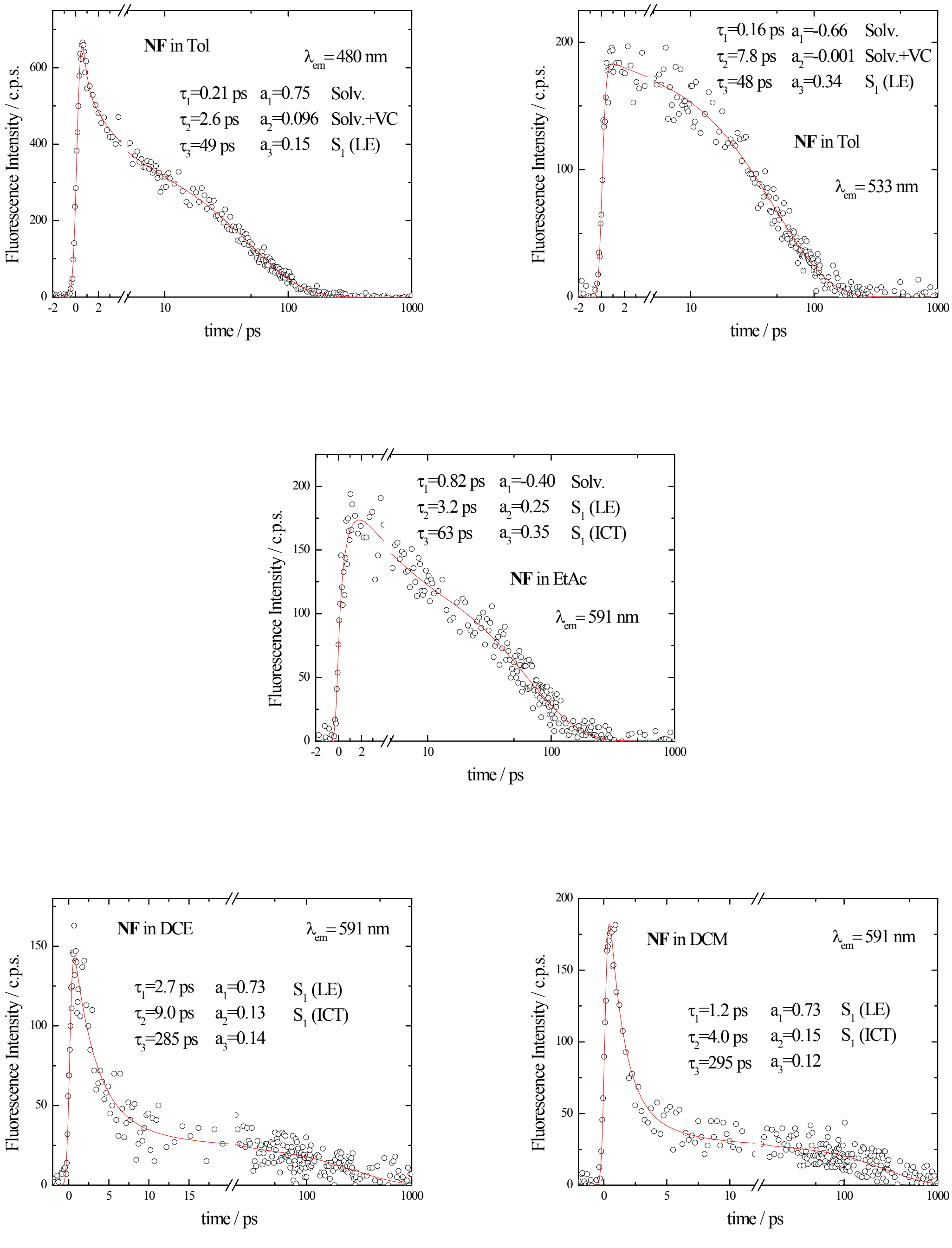

Fig. S21 Decay kinetics recorded at meaningful wavelengths for **NF** in different solvents (the long living component of 285 ps in DCE and 295 ps in DCM, revealed by the fitting of the up conversion kinetics and not previously observed by transient absorption measurements,[7] is probably due to an impurity detected during the emission experiments because of the low fluorescence quantum yield of **NF**).

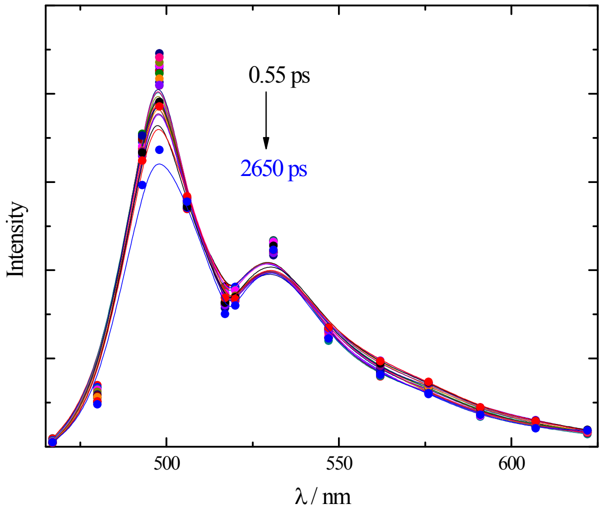

Fig. S22 *TRANES* spectral evolution of **AA** in CH recorded between 0.55 and 2650 ps after the laser pulse.

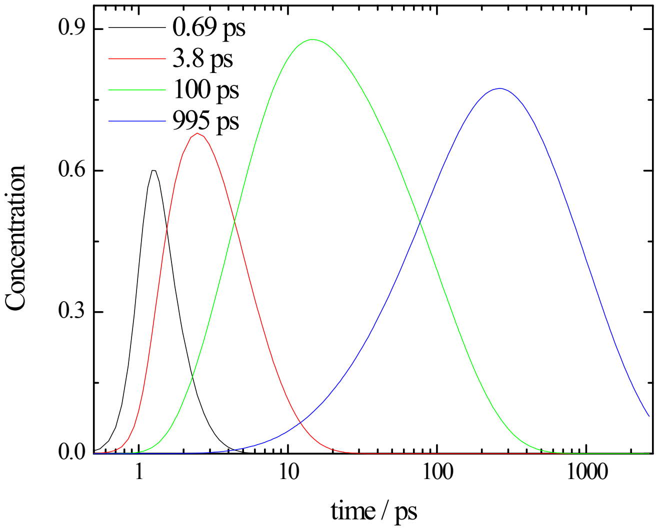

Fig. S23 Concentration profiles of the various transients obtained from the Target Analysis of the fluorescence up-conversion data of **AF** in DCM.

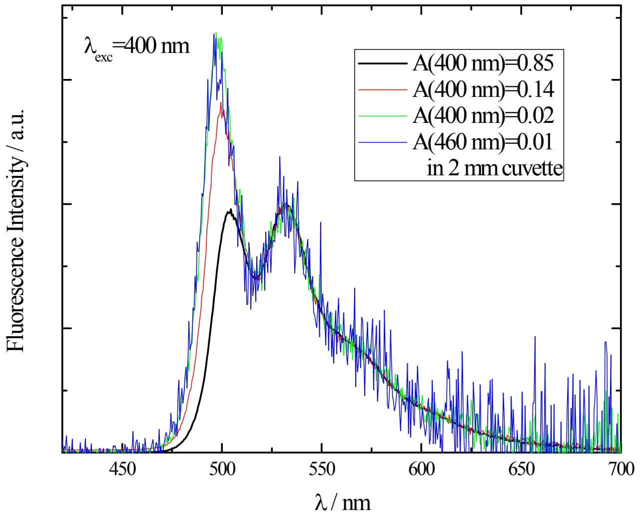

Fig. S24 Steady-state fluorescence emission spectra (recorded in Front Face geometry) of **AA** in CH in solutions of different concentrations (the highest concentration, black spectrum, corresponds to that used during the up-conversion measurements; the lowest concentration, blue spectrum, to that used during the stationary fluorimetric experiments).

Experimental Details.

Single-photon counting measurements and MEM analysis - All the data acquired by single-photon counting method with 0.2 ns resolution, were analyzed by IBH Data Analysis software; the program allows the decay profile of the source from the sample decay to be deconvoluted and provides the fitting of the data, whose goodness is evaluated by means of residuals distribution and the χ2 value. The kinetic traces were also analyzed by means of the Maximum Entropy Method (MEM) by means of the MEMEXP Software available online. In the Maximum Entropy Method the experimental decay I(t) is fitted by the following function:

$$I(t) = D_0 \int_{-\infty}^{+\infty} d\log\tau [g(\log\tau) - h(\log\tau)] \int_{-t_0}^{\min(t,t_f)} dt' R(t') e^{-(t_i - t')/\tau} + \sum_{k=0}^{3} (b_k - c_k) \tag{1}$$

where g(logτ) and h(logτ) are the lifetime distributions that correspond to decay and rise kinetics, respectively, D_0 is a normalization constant, and the polynomial term accounts for the baseline. The instrument response function R(t) is peaked at zero time and is appreciable only in the interval $[-t_0, t_f]$. The fit procedure entails the maximization of the function Q defined in equation (2):

$$Q = S - \lambda C - \alpha I \tag{2}$$

In equation (2), S is entropy defined as:

$$S(\vec{f},\vec{F}) = \sum_{j=1}^{M}[f_j - F_j - f_j \ln(f_j / F_j)] \tag{3}$$

where *f* is the image that includes both the *g* and the *h* lifetime distributions, whereas *F* is the MEM prior distribution used to incorporate prior knowledge into the solution. *C* is a measure of the quality of the fit *F* to the data. When we analyzed the kinetic traces of femtosecond transient absorption with normally distributed noise, *C* was the χ^2. For Poisson-distributed data like those collected by the single photon counting technique, *C* was the Poisson deviance. *I* is a normalization factor; *λ* and *α* are Lagrange multipliers.